MARMARA UNIVERSITY
INSTITUTE FOR GRADUATE STUDIES
IN PURE AND APPLIED SCIENCES

# Rational Design of Molecular Contacts and Defect Analysis in Perovskite Solar Cells

Edina LATIFI

**MASTER THESIS**

Department of Physics

**Thesis Supervisor**

Assoc. Prof. Caner DEGER

ISTANBUL, 2024


# MARMARA UNIVERSITY
## INSTITUTE FOR GRADUATE STUDIES IN PURE AND APPLIED SCIENCES


# Rational Design of Molecular Contacts and Defect Analysis in Perovskite Solar Cells


Edina LATIFI

(521222921)


**MASTER THESIS**

Department of Physics

**Thesis Supervisor**

Assoc. Prof. Caner DEGER

ISTANBUL, 2024

# MARMARA UNIVERSITY
## INSTITUTE FOR GRADUATE STUDIES IN PURE AND APPLIED SCIENCES

Edina LATIFI, a Master of Science student of Marmara University Institute for Graduate Studies in Pure and Applied Sciences, defended her thesis entitled "Rational Design of Molecular Contacts and Defect Analysis in Perovskite Solar Cells", on August 27, 2024 and has been found to be satisfactory by the jury members.

**Jury Members**

Doc.Dr. Caner DEGER
Marmara University .....

Prof. Dr. Mustafa ALEVLI
Marmara Üniversitesi

Doc. Dr. Izzet Parug Duru
Marmara Üniversitesi

## APPROVAL

Marmara University Institute for Graduate Studies in Pure and Applied Sciences Executive Committee approves that Edina LATIFI be granted the degree of Master of Science in Department of Physics Program on August 27, 2024. (Resolution no: ).

# ACKNOWLEDGEMENTS

First and foremost, I am deeply thankful to Allah for granting me the health, determination, and opportunity to complete this thesis. His blessings have been the foundation of all my efforts. I would like to express my profound gratitude to my supervisor, Professor Caner DEGER, for his exceptional guidance, steadfast support, and generosity throughout this journey. I am especially grateful for the inspiring and professional research environment he cultivated, as well as his dedication to providing high-quality education and mentorship. His influence has been pivotal in my academic growth and in bringing this work to fruition. My heartfelt thanks go to Ilhan Yavuz, Muratcan Oner, and Dogukan Acıkgoz for their valuable contributions and for generously sharing their extensive knowledge with enthusiasm. Their input has been instrumental in shaping this research. I am also thankful to my colleagues at Simulab for their collaboration and support, which have significantly aided the progress of this study. Lastly, I wish to extend my deepest thanks to my family and friends. Their unwavering encouragement, love, and patience have been my greatest sources of strength throughout this endeavor.

**August, 2024** **Edina LATIFI**

# CONTENTS

PAGE

**ACKNOWLEDGEMENTS** . . . . . **i**

**TABLE OF CONTENTS** . . . . . **ii**

**ÖZET** . . . . . **iii**

**ABSTRACT** . . . . . **iv**

**SYMBOLS** . . . . . **v**

**ABBREVIATIONS** . . . . . **vii**

**1 INTRODUCTION** . . . . . **1**

**2 METHODS** . . . . . **6**

2.1 Density Functional Theory . . . . . 6

2.2 Computational Details for Rational Design of Self-Assembled Monolayers toward Efficient and Stable Perovskite Solar Cells . . . . . 12

2.3 Computational Details for Formation of Surface Defects in Lead-Free Tin Halide Perovskites . . . . . 13

**3 RESULTS AND DISCUSSION** . . . . . **15**

3.1 Rational Design of Self-Assembled Monolayers toward Efficient and Stable Perovskite Solar Cells . . . . . 15

3.1.1 Candidate Molecules . . . . . 15

3.1.2 Molecule-ITO and Molecule-Perovskite interaction . . . . . 19

3.1.3 Stacking Energy . . . . . 24

3.1.4 Charge Transfer Properties . . . . . 25

3.2 Formation of Surface Defects in Lead-Free Tin Halide Perovskites . . 29

3.3 Publications . . . . . 32

**4 CONCLUSION** . . . . . **33**

# ÖZET

**Güneş hücrelerinde moleküler temas, farklı malzemelerin moleküler düzeyde buluştuğu ve etkileşime girdiği arayüzü ifade eder; bu temas, verimli yük transferi için kritik öneme sahiptir. Zayıf temaslar enerji kayıplarına yol açarak hücrenin verimliliğini azaltabilir. Son zamanlarda rapor edilen sofistike tek katmanlar için Py3 molekülünün üst kısmını, çeşitli atom ve moleküller ekleyip bağlayarak Py3'ün birkaç hesaplamalı türevini oluşturmak amacıyla değiştirdik. On iki farklı modifikasyonun kapsamlı bir analizini yaparak, bu moleküllerin katmanlar arasında farklı davranışlar sergilediğini gözlemledik. 2-(5-aminopyren-1-yl)ethyl)phosphonic acid molekülü, perovskit katmanı ile en yüksek etkileşimi gösterdi. Eklenen atom veya moleküle bağlı olarak, perovskit katmanı ile etkileşimler değişti ve bu süreçte yalnızca daha stabil bir moleküler kontak tabakası elde etmekle kalmayıp, aynı zamanda ITO-Perovskit arasındaki yük transferini arttırmayı hedefledik. Paralel olarak, kurşunsuz alternatifler olarak formamidinyum kalay iyodür (FASnI3), metilamonyum kalay iyodür (MASnI3) ve karışık katyon formamidinyum-metilamonyum kalay iyodür (FAMASnI3) perovskit malzemelerde yüzey kusur oluşumlarını inceledik. Cihaz performansını olumsuz etkileyebilecek kusurları belirlemek amacıyla, boşluklar, arayer atomları ve antisite gibi geniş bir kusur yapısını sistematik olarak araştırdık. Özellikle, iyot arayer atomları, FA antisitesi ve iyot boşluklarının düşük oluşum enerjilerine sahip zararlı kusurlar olduğunu tespit ettik.**

# ABSTRACT

**Molecular contact in solar cells refers to the interface where different materials meet and interact at the molecular level, crucial for efficient charge transfer. Poor contacts can lead to energy losses, reducing the cell's efficiency. In a result for sofisticaded monolayers Py3 was lately reported, we modified the top portion of Py3, a recently reported interface molecule, by adding and bonding different atoms and molecules to create several computational derivatives of Py3. Through a comprehensive analysis of twelve distinct modifications, we observed varying behaviors of these molecules between layers, with the 2-(5-aminopyren-1-yl)ethyl)phosphonic acid molecule demonstrating the highest interaction with the perovskite layer. Depending on the inserted atoms or molecules, the interactions with the perovskite layer changed, aiming not only to improve the stability but also to achieve an enhanced charge transfer between ITO and Perovskite layers. In parallel, we examined surface defect formations in formamidinium tin iodide (FASnI3), methylammonium tin iodide (MASnI3), and mixed cation formamidinium-methylammonium tin iodide (FAMASnI3) perovskite materials as lead-free alternatives. We systematically investigated a wide range of defect structures, including vacancies, interstitials, and antisites, to identify detrimental defects that could impact device performance. Notably, we found that iodine interstitials, FA antisites, and iodine vacancies are harmful defects with low formation energies.**

.

# SYMBOLS

| | |
|---|---|
| $\boldsymbol{T_f}$ | : Goldschmidt's tolerance factor |
| $\boldsymbol{R_A}$ | : Ionic radii of the A ion |
| $\boldsymbol{R_B}$ | : Ionic radii of the B ion |
| $\boldsymbol{R_X}$ | : Ionic radii of the X ion |
| $\boldsymbol{V_x}$ | : Vacancy of X atom or molecule |
| $\boldsymbol{X_{int}}$ | : Interstial of X atom |
| $\boldsymbol{E_{tot}}$ | : Total energy of many electron system |
| $\boldsymbol{\Psi}$ | : The many-body wave function of the system |
| $\boldsymbol{\hat{H}}$ | : Hamiltonian of the system |
| $\boldsymbol{\hat{T}}$ | : Kinetic energy |
| $\boldsymbol{\hat{Z}}$ | : Coloumb energy |
| $\boldsymbol{V_m}$ | : External potential energy |
| $\mathbf{r}_i$ | : Position vector of ith electron |
| $\boldsymbol{\nabla^2}$ | : Laplace operator |
| $\boldsymbol{F[X]}$ | : Functional of function X |
| $\langle$ | : Bra |
| $\rangle$ | : Ket |
| $\boldsymbol{E_{XC}}$ | : Exchange-correlation energy |
| $\boldsymbol{n}(\mathbf{r})$ | : Electron density |
| $\boldsymbol{n_o}$ | : Ground state electron density |
| $\boldsymbol{V_H}$ | : Hartree potential |
| $\boldsymbol{V_{tot}}$ | : Effective potential |
| $\boldsymbol{V_{XC}}$ | : Exchange-correlation potential |
| $\boldsymbol{\varepsilon_i}$ | : Eigen vectors |
| $\boldsymbol{\psi_i}(\mathbf{r})$ | : Eigen values |
| $\boldsymbol{c_i}(\mathbf{G})$ | : Plane-wave coefficients |
| $\mathbf{G}$ | : Reciprocal lattice vector |

$\mathbf{G}_{max}$ : Biggest reciprocal lattice vector in series expansion

$\varepsilon_{xc}$ : Exchange-correlation energy approximation

$E_{XC}^{LDA}$ : Exchange-correlation energy functional with local density approximation

$E_{XC}^{GGA}$ : Exchange-correlation energy functional with generalized gradient approximation

$E_{XC}^{meta-GGA}$ : Exchange-correlation energy functional with meta-generalized gradient approximation

$E_{cut}$ : Cutoff energy

$E_F$ : Fermi energy

$E_{VBM}$ : Energy of the valence band maximum

$\vec{G}$ : Reciprocal lattice vector

$n_i$ : Number of atoms added or substracted

$\Delta H^{FE}(D)$ : The formation energy of doped system

$E_{tot}(B)$ : Total energy of the pristine supercell

$E_{tot}(D)$ : Total energy of the doped supercell

$E_f$ : Fermi level energy

$E_{VBM}$ : Valence band maximum energy

$E_{corr}^{q}$ : Finite size correction energy

$\Delta V$ : Potential alignment term

$\mu_i$ : Total chemical potential of atom/compound i

$\mu_i'$ : Energy of one atom/compound

$\Delta\mu_i$ : Intrinsic chemical potential of atom/compound i

$n_i$ : Number of kind i atoms removed from or added to the pristine structure

$q$ : Charge

# ABBREVIATIONS

| | |
|---|---|
| SAM | : Self Assembled Monolayers |
| ITO | : Indium Tin Oxide |
| DFT | : Density Functional Theory |
| CDD | : Charge density Difference |
| CTP | : Charge Transport Properties |
| PSC | : Perovskite Solar Cell |
| ETL | : Electron Transport Layer |
| HTL | : Hole Transport Layer |
| LDA | : Local Density Approximation |
| OSC | : Organic Semiconductor |
| GGA | : Generalized Gradient Approximation |
| PV | : Photovoltaic |
| PCE | : Power Conversion Efficiency |

# 1. INTRODUCTION

The global demand for energy has been steadily increasing over the past decades, driven by rapid population growth, industrialization, and the pursuit of higher living standards. According to the International Energy Agency (IEA), the world's energy demand is expected to rise by approximately 25% by 2040, with much of this growth concentrated in developing economies [1]. This surge in energy consumption presents significant challenges, particularly in the context of environmental sustainability and climate change. Currently, fossil fuels, including coal, oil, and natural gas, dominate the global energy landscape, supplying about 80% of the world's energy needs [2]. However, the extensive use of these energy sources has led to severe environmental consequences, including air pollution, greenhouse gas emissions, and global warming [3]. As a result, there is an urgent need to transition to renewable energy sources that can meet the growing energy demand while minimizing environmental impact. Solar energy, one of the most abundant and cleanest renewable energy sources, has emerged as a key player in the global effort to reduce reliance on fossil fuels. The sun provides an immense amount of energy, with estimates suggesting that the amount of solar energy reaching the Earth's surface in one hour is sufficient to meet the world's energy needs for an entire year [4]. Harnessing this energy through PV technology has thus become a central focus of research and development in the renewable energy sector. Traditional silicon-based solar cells have dominated the photovoltaic market for decades due to their relatively high efficiency and stability. However, the high production costs and energy-intensive manufacturing processes associated with silicon photovoltaics have spurred interest in alternative materials that can offer similar or better performance at lower costs [5]. Among these alternatives, PSCs have garnered significant attention over the past decade. The rapid development of perovskite-based materials has revolutionized the field of photovoltaic research, positioning PSCs as one of the most promising technologies for next-generation solar energy conversion. The journey of perovskites from obscurity to the forefront of photovoltaic innovation is a testament to the remarkable versatility and potential of

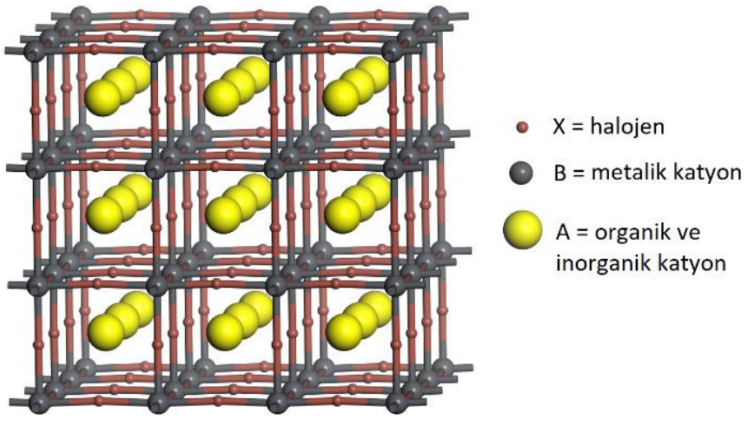


**Figure** 1.1 Perovskite crysral structure.

these materials [6]. Perovskites, originally discovered in 1839 by Russian mineralogist Lev Perovski in the Ural Mountains, were initially recognized for their unique crystal structure, characterized by the general formula $ABX_3$, where 'A' and 'B' are cations and 'X' is an anion. This structure, which allows for a wide range of chemical substitutions, grants perovskites a remarkable degree of tunability in their physical and chemical properties [7]. For decades, perovskites were primarily of interest in fields such as catalysis, ferroelectrics, and superconductivity, but their potential as a light-harvesting material in photovoltaic devices remained unexplored until much later. The modern era of perovskite research in photovoltaics began in 2009 when a group of researchers led by Tsutomu Miyasaka at Toin University of Yokohama first demonstrated the use of a perovskite material as a light absorber in a dye-sensitized solar cell (DSSC) [8]. Although the initial efficiency of around 3.8 % was modest, this study marked a pivotal moment, introducing the scientific community to the potential of perovskites in solar energy conversion. These early efforts were focused on the use of organic-inorganic lead halide perovskites, which exhibited promising optoelectronic properties but suffered from poor stability due to the use of a liquid electrolyte in the device structure [9]. The true breakthrough in perovskite solar cells came in 2012 when researchers successfully replaced the liquid electrolyte with a solid-state hole transport material, leading to significant improvements in both the efficiency and stability of the devices. This innovation sparked a rapid surge in research and development, propelling perovskite solar cells from laboratory curiosities

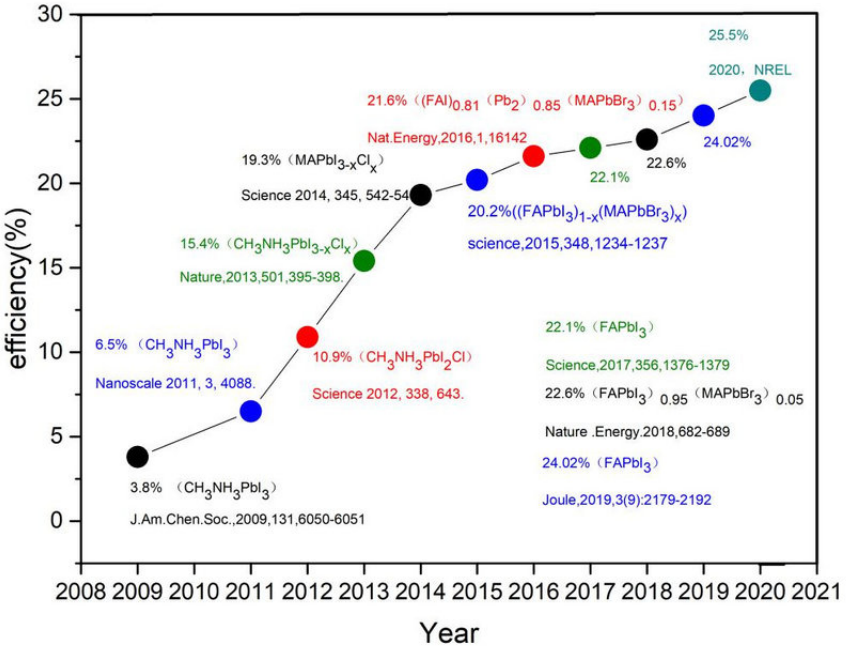


**Figure** 1.2 Graph showing the rapid growth of PVC efficiency in the latest years. [11]

to serious contenders in the race for high-efficiency, low-cost photovoltaic technologies. Within just a few years, the power PCE of perovskite solar cells increased dramatically, surpassing 10% by 2012, 20% by 2014, and reaching over 25% in recent laboratory demonstrations. This meteoric rise in efficiency, combined with the relatively low cost of materials and ease of fabrication, has positioned perovskites as a leading candidate for the next generation of solar cells, capable of rivaling and even surpassing traditional silicon-based technologies [10]. The exceptional performance of perovskite solar cells can be attributed to several key factors, including their high absorption coefficients, tunable bandgaps, long carrier diffusion lengths, and low exciton binding energies. These properties enable efficient light absorption, charge separation, and charge transport within the perovskite layer, which is typically sandwiched between electron transport layers (ETL) and hole transport layers (HTL) in a solar cell architecture [12]. The quality of the interfaces between the perovskite layer and the transport layers is critical for optimizing device performance. Poorly managed interfaces can lead to significant energy losses, charge recombination, and reduced device stability [13]. To address these challenges, various strategies have been developed, with one of the most promising being the use

of self-assembled monolayers (SAMs). SAMs are two-dimensional nanomaterials that can modify electrode surfaces by forming organized molecular structures that improve charge injection or extraction at the interfaces [14]. The incorporation of SAMs has been shown to significantly enhance the performance and stability of perovskite solar cells by reducing trap densities and improving the electronic properties of the interfaces. These improvements are crucial for achieving high-efficiency devices that can maintain their performance over extended periods [15].

Despite the impressive progress made with lead-based perovskites, the inherent toxicity and environmental concerns associated with lead have spurred an urgent search for lead-free alternatives. The widespread adoption of lead-based perovskite solar cells is hindered by the potential environmental and health risks posed by lead, particularly in the event of material degradation or improper disposal. This has become a major area of focus within the perovskite research community, as the long-term sustainability of PSCs depends on finding materials that can deliver similar or better performance without the associated risks of lead [16]. Among the lead-free candidates, tin halide perovskites have garnered significant attention due to their similar optoelectronic properties to lead-based perovskites. Tin halide perovskites, particularly those incorporating formamidinium (FA) and methylammonium (MA) cations, have shown promise as viable alternatives, offering comparable bandgaps and charge transport properties. However, one of the critical challenges in their application is the formation of surface defects, which can significantly impact the performance and stability of these materials. Surface defects, such as vacancies, interstitials, and antisites, create deep trap states within the bandgap, adversely affecting charge carrier dynamics and leading to recombination losses. These defects not only reduce the efficiency of tin-based perovskite solar cells but also contribute to their rapid degradation under operational conditions, posing a significant barrier to their commercial viability [17]. To address these challenges, a deeper understanding of the nature of surface defects in tin halide perovskites and the development of effective strategies for their passivation are essential. Research has shown that the stability and electronic properties of these materials are highly dependent on

their surface termination and the surrounding growth conditions. For instance, $SnI_2$-terminated surfaces exhibit a higher tolerance to defect formation, suggesting that careful control of surface termination could be a viable strategy for improving the stability of tin halide perovskites. Additionally, the exploration of mixed-cation tin halide perovskites, such as those combining FA and MA cations, offers potential pathways for optimizing the material's properties by balancing the trade-offs between stability and performance [18].

Despite the differences between lead-based and lead-free perovskites, both systems share common challenges related to defect management and interfacial optimization. In lead-based perovskites, significant efforts have been directed towards enhancing the quality of the perovskite/ETL and perovskite/HTL interfaces through the incorporation of SAMs and other molecular modifications. These strategies aim to create well-matched energy levels and reduce non-radiative recombination losses, thereby improving device efficiency and stability. For instance, the use of SAMs has been shown to effectively passivate surface defects and improve the alignment of energy levels at the interfaces, leading to more efficient charge transfer and reduced recombination losses. In contrast, lead-free perovskites, particularly tin-based variants, require a deeper understanding of intrinsic defect formation and the development of passivation techniques to mitigate the impact of surface defects on carrier dynamics. The challenges associated with tin-based perovskites are compounded by their higher sensitivity to oxidation and other environmental factors, which can exacerbate defect formation and accelerate material degradation. Therefore, developing robust passivation strategies and optimizing growth conditions are critical to unlocking the full potential of tin-based perovskites for photovoltaic applications [19]. This study seeks to integrate the insights and methodologies from both lead-based and lead-free perovskite research to develop a comprehensive approach to improving perovskite solar cell performance. By combining the use of SAMs and other interfacial engineering techniques from lead-based systems with defect passivation strategies from lead-free systems, we aim to address the challenges of both material classes. Specifically, we will explore the potential of novel SAMs to

enhance the electronic properties of tin halide perovskites, focusing on minimizing surface defects and improving charge transport across interfaces. Furthermore, we will investigate the effects of various growth conditions and surface terminations on the stability and electronic properties of tin halide perovskites, with the goal of identifying optimal fabrication processes that minimize defect formation. Through this multidisciplinary approach, we hope to advance the development of more stable, efficient, and environmentally friendly perovskite solar cells [14]. By bridging the gap between lead-based and lead-free perovskite research, our work will contribute to the broader effort of creating sustainable and high-performance optoelectronic devices that can meet the growing global demand for renewable energy solutions. The insights gained from this research will not only enhance our understanding of perovskite materials but also pave the way for the development of new strategies to overcome the current limitations of perovskite solar cells, ultimately bringing us closer to realizing the full potential of this promising technology. As the world faces increasing pressures to transition to renewable energy sources, the development of efficient, cost-effective, and environmentally friendly solar technologies like perovskite solar cells will play a crucial role in shaping the future of global energy production.

# 2. METHODS

## 2.1. Density Functional Theory

Density Functional Theory is a computational quantum mechanical modeling method that has become indispensable in the fields of chemistry, physics, and materials science. It is used to study the electronic structure of atoms, molecules, and condensed matter systems. The appeal of DFT lies in its ability to provide a good balance between accuracy and computational efficiency, making it suitable for a wide range of applications. The fundamental principle of DFT is rooted in the idea that the properties of a many-electron system can be uniquely determined by its electron density, rather than by the many-body wavefunction, which is much more complex

to handle. This concept was first formalized by Hohenberg and Kohn in 1964, who proved that the ground state energy of a system is a unique functional of the electron density [20]. This was a groundbreaking realization because it shifted the focus from solving the Schrödinger equation for the wavefunction, a task that becomes increasingly difficult as the number of electrons increases, to a more manageable problem involving the electron density. The Kohn-Sham formalism, introduced by Kohn and Sham in 1965, further developed DFT by introducing a system of non-interacting particles that have the same electron density as the interacting system of interest [21]. This approach allowed for the practical implementation of DFT, making it feasible to calculate the properties of real systems. A key component of this approach is the exchange-correlation functional, which accounts for the complex many-body interactions, including both exchange and correlation effects between electrons. However, the exact form of the exchange-correlation functional is unknown, and various approximations are used, such as the Local Density Approximation (LDA) and the GGA [22]. DFT has been successfully applied to a wide variety of problems, from calculating the electronic structure of molecules to predicting the properties of new materials. Its versatility and efficiency have made it a standard tool in computational material science and chemistry. However, DFT is not without limitations. The accuracy of DFT calculations depends heavily on the choice of the exchange-correlation functional, and some systems, such as those with strong electron correlation effects, are challenging for standard DFT approaches [23]. Despite these challenges, ongoing research continues to refine and extend the capabilities of DFT, ensuring its continued relevance in the study of complex systems. The electronic configuration of a material provides crucial information about its characteristics. Examining the electron ground state allows for the comprehension of the material's stability, vibrational dynamics, and insulating properties. Therefore, precise knowledge of electronic structures is vital. The total energy $E_{tot}$ of a system with multiple electrons can be determined using Equation 2.1, where $\Psi$ represents the many-body wave function and $\hat{H}$ denotes the system's Hamiltonian.

$$E_{tot} = \langle \Psi | \hat{H} | \Psi \rangle = \int d\mathbf{r}_1 ... d\mathbf{r}_M \Psi^*(\mathbf{r}_1, ..., \mathbf{r}_M) \hat{H} \Psi(\mathbf{r}_1, ..., \mathbf{r}_M). \tag{2.1}$$

The Hamiltonian for a system with multiple electrons can be represented in Equation 2.2, which is then simplified into a more concise expression in Equation 2.3.:

$$\hat{H}(\mathbf{r}_1, \mathbf{r}_2, ..., \mathbf{r}_M) = \underbrace{-\sum_j \frac{1}{2}\nabla_i^2}_{\hat{T},\ \text{Kinetic energy}} + \underbrace{\sum_j V_m(\mathbf{r}_i)}_{\text{External potential}} + \underbrace{\frac{1}{2}\sum_{j \neq i} \frac{1}{|\mathbf{r}_i - \mathbf{r}_i|}}_{\hat{Z},\ \text{Coulomb energy}}, \tag{2.2}$$

$$E_{tot} = \langle \Psi | \sum_i V_m(\mathbf{r}_i) | \Psi \rangle + \langle \Psi | \hat{T} + \hat{Z} | \Psi \rangle . \tag{2.3}$$

DFT represents a computational approach that relies on the electron probability density rather than the traditional wave function used in quantum mechanics. This method was initially proposed by Hohenberg and Kohn in their seminal 1964 paper. However, it wasn't until the development of high-performance supercomputers that DFT became a fundamental tool in materials science, enabling researchers to perform complex calculations that were previously impractical.

The foundational idea behind DFT is rooted in the work of Hohenberg and Kohn, which revolutionized the way scientists approach the study of many-electron systems. The theory allows us to express the total energy $E_{tot}$ of such a system as a functional of the wave function $\Psi$, mathematically represented as $E_{tot} = F[\Psi]$. This relationship highlights that the total energy $E_{tot}$ is inherently dependent on the many-body wave function $\Psi$, which governs the behavior of electrons within the system. The theorem derived by Hohenberg and Kohn establishes several key principles: External Nuclear Potential Determination**: The ground state electron density $n$ uniquely determines the external potential $V_m$ exerted by the nuclei. This relationship is crucial because it indicates that the electron density alone contains all the necessary information about the external forces acting on the electrons, as

expressed in Equation 2.2. Wave Function Uniqueness**: The wave function $\Psi$ of the system is uniquely determined by the external potential $V_m$ in any state, whether it is the ground state or an excited state. This implies that once the external potential is known, the wave function can be precisely calculated, and therefore, the behavior of the entire electron system can be predicted. Energy as a Functional**: The total energy $E_{tot}$ of the system can be described as a functional of the many-body wave function $\Psi$ across any state, as highlighted in Equation 2.1. This functional relationship is central to DFT, as it simplifies the calculation of total energy by focusing on the wave function's dependencies. By combining these principles, we arrive at a critical conclusion: the ground state electron density $n$ uniquely determines the total energy $E_{tot}$. In other words, the total energy of a system can be expressed as a functional of the electron density, $E_{tot} = F[n]$. This insight is fundamental to DFT, as it shifts the focus from the complex many-body wave function to the more manageable electron density, making it a powerful tool for analyzing and predicting the properties of materials.

$$E_{tot} = F[n(\mathbf{r})] = \int d\mathbf{r} n(\mathbf{r}) V_m(\mathbf{r}) + \langle \Psi[n] | \hat{T} + \hat{Z} | \Psi[n] \rangle \,. \tag{2.4}$$

In this context, $\hat{T}$ and $\hat{Z}$ denote the kinetic and Coulomb energies, respectively, with their dependence on $n$ being implied rather than explicitly stated. However, the first term in the functional directly depends on $n$. In 1965, Kohn and Sham refined the original formulation by separating the implicit components into kinetic energy and the Hartree potential for non-interacting electrons. They also introduced an additional term, $E_{xc}$, to account for exchange and correlation energy. While the precise form of this functional is still unknown, various useful approximations have been developed since the foundational work of Hohenberg and Kohn.

Equation 2.5 is essentially a reformulation of Equation 2.4:

$$E_{tot} = \overbrace{\underbrace{\int d\mathbf{r} n(\mathbf{r}) V_m(\mathbf{r})}_{\text{External potential}} - \underbrace{\sum_j \int d\mathbf{r} \phi_j^*(\mathbf{r}) \frac{\nabla^2}{2} \phi_j(\mathbf{r})}_{\text{Kinetic energy}} + \underbrace{\frac{1}{2} \iint d\mathbf{r} d\mathbf{r}' \frac{n(\mathbf{r}) n(\mathbf{r}')}{|\mathbf{r} - \mathbf{r}'|}}_{\text{Hartree potential}}}^{\text{The independent electron approximation energy}} + \underbrace{E_{xc}[n]}_{\text{XC energy}} . \tag{2.5}$$

To calculate the total energy $E_{tot}$ of the system, we apply the relation $E_{tot} = F[n]$, which is based on the electron density $n$. The electron density is obtained using the Hohenberg-Kohn variational principle, which asserts that the ground state density $n_0$ minimizes $E_{tot} = F[n]$. This principle results in the formulation of the Kohn-Sham equations:

$$\left[ -\frac{1}{2}\nabla^2 + V_{tot}(\mathbf{r}) \right] \psi_j(\mathbf{r}) = \varepsilon_j \psi_j(\mathbf{r}), \tag{2.6}$$

$$V_{tot}(\mathbf{r}) = V_m(\mathbf{r}) + V_H(\mathbf{r}) + V_{xc}(\mathbf{r}). \tag{2.7}$$

In periodic systems such as crystal structures, the Kohn-Sham wavefunctions can be represented using a plane wave basis to enhance computational efficiency.:

$$\psi_j(\mathbf{r}) = \sum_{\mathbf{G}} c_j(\mathbf{G}) \exp^{(i\mathbf{G}\cdot\mathbf{r})}, \tag{2.8}$$

In this context, $\psi_j(\mathbf{r})$ is expressed as a linear combination of plane waves that adhere to periodic boundary conditions. The vectors $\mathbf{G}$ correspond to the reciprocal lattice vectors. Although the summation can theoretically involve an infinite number of terms, only a finite number of $\mathbf{G}$ vectors are actually used, forming a series. The maximum $\mathbf{G}$ vector in this series determines the level of detail in the calculation. The collection of all plane waves in the series is referred to as the basis set, with the cutoff for the plane waves defined by:

$$E_{cut} = \frac{\left|\mathbf{G}_{max}\right|^2}{2}. \tag{2.9}$$

In the independent electron model, the electron charge density $n(\mathbf{r})$ is calculated by aggregating the probabilities of locating electrons in each filled state $j$.:

$$n(\mathbf{r}) = \sum_{j}^{N} \left|\psi_j(\mathbf{r})\right|^2. \tag{2.10}$$

By reformulating Equation 2.7 with the plane wave representation provided in Equation 2.8, we obtain:

$$\frac{\left|\mathbf{G}^2\right|}{2} c_j(\mathbf{G}) + \sum_{\mathbf{G}'} v_{tot}(\mathbf{G} - \mathbf{G}') c_j(\mathbf{G}') = \varepsilon_j c_j(\mathbf{G}), \tag{2.11}$$

These are the Kohn-Sham equations, which can be resolved through iterative self-consistent calculations until the desired level of accuracy is reached [24].

## 2.2. Computational Details for Rational Design of Self-Assembled Monolayers toward Efficient and Stable Perovskite Solar Cells

We carried out the computational aspect of this study using density functional theory (DFT) and first-principles calculations. The VASP software [25,26] was utilized, employing a plane-wave basis set and the projected augmented wave (PAW) method. For the exchange-correlation functional, we used the Perdew-Burke-ErnzDuring the geometry optimizations, a $4 \times 4 \times 1$ $\Gamma$ -centered k-mesh was applied, and the energy cutoff for the plane-wave basis was set at 400 eV. Atomic positions and cell volumes were carefully relaxed using until the forces wore less than 0.03 eV/Å. Additionally, a vacuum slab with a thickness of 10-15 Å was introduced between the periodic slab-molecule structure along the z-axis. The optimized geometry of the perovskite-molecule interface was used to determine the molecular stacking energy. This was done by first calculating the total energy of the OSC layer, which consisted of 2 molecules, then calculating the free energy of the isolated molecules. The molecular stacking energy was obtained by subtracting the free energy of the 2 isolated molecules from the total energy of the OSC layer.

## 2.3. Computational Details for Formation of Surface Defects in Lead-Free Tin Halide Perovskites

We performed first-principles calculations by using DFT with plane-wave basis set and the projected augmented wave (PAW) method within the Vienna Ab initio Simulation Package (VASP) [25,26]. For all geometry optimizations, revised Perdew-Burke-Ernzerhof (PBEsol) [27]for solids and surfaces is used as Generalized-gradient-approximation GGA functional. For self consistent calculations, range separated HSE06 [28] hybrid functional is also performed consecutively to PBEsol with the inclusion of spin-orbit coupling (SOC) [29] . The overall calculation procedure is PBEsol+HSE06 with SOC included. A plane-wave basis with 400 eV kinetic energy cutoff is used. 4 x 4 x 1 Γ-centered k-mesh is used for geometry optimizations. Site positions were allowed to relax until all residual forces are smaller than 0.01 eV/Å. All perovskite layers for computing formation energies are konsrtructed along [001] growth direction. We considered 3 different types of terminations: (i) I-terminated, (ii) $SnI_2$-terminated, and (iii) AI-terminated surfaces, where A can be FA, MA, FAMA (see Figure 1). Surface formation energies are calculated (See SI for detail).

Subsequently, we investigate intrinsic point defects as introduced on one side of the slabs, including vacancies ($V_X$), anti-site defects ($X_Y$), and interstitial defects ($X_i$). The formation energies of the relaxed slabs with these defects are calculated using the following formula:

$$\Delta H_q^d = E_q^d - E_{\mathrm{pr}} + \sum_i X_{\mathrm{ini}}\mu_i + q(E_F + E_{\mathrm{VBM}}) + E_{\mathrm{corr}} \tag{2.12}$$

Here, q and d denote the charge state and defect type, respectively. Epr represents the energy of the pristine slab, and ni refers to the change in the number of elements exchanged from the reservoir to form the corresponding defect. $\mu_i$, $E_F$ , and $E_{VBM}$ stand for the chemical potential, Fermi energy, and valence-band maximum energy, respectively. $E_{corr}$ is the energy correction applied due to the finite

sizes of the super-cells considered in the formation energy calculations. The chemical potentials of Sn, I, FA, and MA are calculated from

$$\mu = \mu_0 + \Delta\mu_0 \tag{2.13}$$

where $\mu_0$ denotes the "intrinsic" chemical potential, derived from the stable cell energy of the material, and $\Delta\mu$ represents the "external" chemical potential, which varies based on environmental (growth) conditions. The permissible values for the external chemical potentials of Sn, I, FA, and MA, relevant for the formation of $FASnI_3$, $MASnI_3$, and $FAMASnI_3$ under thermal equilibrium, are determined by adapting the methodology from Yin et al. [30].

# 3. RESULTS AND DISCUSSION

## 3.1. Rational Design of Self-Assembled Monolayers toward Efficient and Stable Perovskite Solar Cells

### 3.1.1. Candidate Molecules

Figure 3.1 shows a 3 layered crystal representing solar cell structure, and a series of molecules which are designed to fit the middle layer of the crystal and often adressed self assembled monolayers or lately called molecular contact part. Figure. 3.1 a) illustrates an intricately designed multilayer architecture consisting of $FAPbI_3$ perovskite, a Py3 SAM, and ITO. Each layer is depicted with a precise color-coded scheme to facilitate understanding of the structural and functional relationships. The top layer showcases $FAPbI_3$, a lead halide perovskite renowned for its outstanding optoelectronic properties, which are critical in the field of photovoltaic technology [31]:

Lead (Pb) atoms, represented in dark gray, form the central framework of the perovskite lattice. This structure provides the necessary pathways for electron transport, significantly contributing to the material's high carrier mobility [32]. Iodine (I) atoms, shown in purple, are crucial for completing the octahedral configuration around the lead atoms. This arrangement facilitates efficient charge separation and transport, minimizing losses due to recombination. Formamidinium (FA) ions, composed of carbon (C) in orange, nitrogen (N) in blue, and hydrogen (H) in light pink, are interspersed within the lattice. These organic cations play a pivotal role in stabilizing the perovskite structure, influencing both the bandgap and the thermal stability of the material [33]. The perovskite's crystalline lattice is known for its remarkable light absorption capabilities across the visible spectrum, which is essential for generating a high photocurrent. Its unique structural properties allow for the facile tuning of electronic and optical characteristics, making it a versatile material

in the development of high-efficiency solar cells [34].

As for the middle layer Py3 as a SAM is strategically placed beneath the perovskite layer, serving as a crucial interface modifier that enhances the device's overall performance: Carbon (C) atoms in orange form the backbone of the SAM, providing structural integrity and flexibility. Nitrogen (N) atoms, depicted in blue, contribute to the electronic functionality and chemical reactivity of the SAM, facilitating interactions with other layers. Hydrogen (H) atoms, shown in light pink, engage in hydrogen bonding, which can further stabilize the interface and reduce defect densities. Phosphorous (P) atoms, shown in dark purple and the oxygen atoms (O) shown in red form the phosphonic acid part which bonds the SAM molecule to the ITO layer. The Py3 SAM acts as a passivation layer, effectively reducing surface defects and mitigating the formation of trap states that could otherwise hinder charge carrier mobility. By improving the alignment of energy levels between the perovskite and the ITO, the SAM plays a critical role in enhancing charge transfer efficiency. This optimization is essential for reducing recombination rates and increasing the

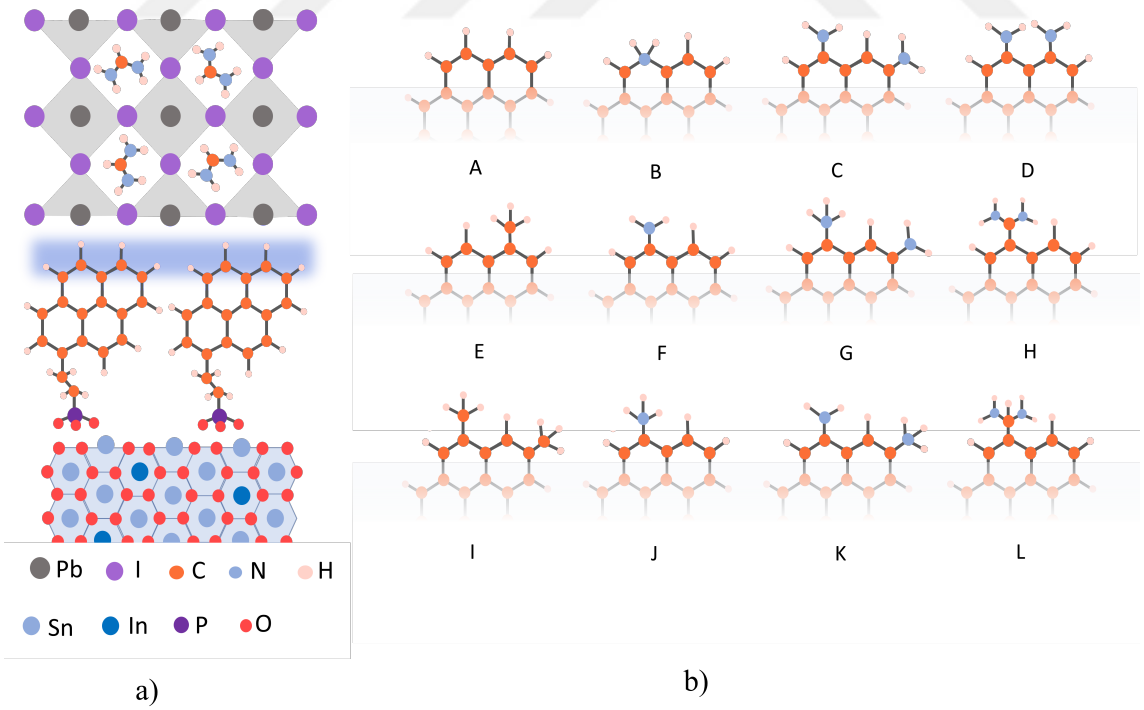


**Figure** 3.1 a) The crystal structure of three layers, b) Py3 derived molecules and their structure.

device's fill factor and open-circuit voltage. The chemical and physical stability provided by the SAM contributes to the longevity and reliability of the solar cell under operational conditions [35]. When it comes to the bottom Layer ITO forms the base of the structure, offering a combination of transparency and conductivity that is indispensable for the function of optoelectronic devices: Tin (Sn) atoms in light blue and Indium (In) atoms in dark blue collectively form a conductive network that supports efficient charge collection and transport [36]. Oxygen (O) atoms, depicted in red, are integral to maintaining the structural and electronic properties of the ITO layer, ensuring stability and performance. ITO is widely utilized in photovoltaic applications due to its excellent electrical conductivity paired with optical transparency, allowing for efficient light penetration and charge collection.The optimization of ITO's properties, such as surface morphology and work function, is crucial for minimizing resistive losses and achieving high power conversion efficiencies. The interactions between these layers are meticulously engineered to maximize device performance. The Py3 SAM not only enhances the electronic interface but also provides a robust chemical barrier, protecting the perovskite layer from environmental degradation. This careful design minimizes charge carrier recombination and ensures efficient charge extraction, critical for achieving high power conversion efficiencies [37]. In conclusion, the multilayer structure exemplifies a sophisticated integration of materials, each contributing distinct yet complementary properties to the overall device. By leveraging the unique characteristics of $FAPbI_3$, Py3 SAM, and ITO, this architecture achieves enhanced efficiency, improved stability, and scalability potential, representing a significant advancement in photovoltaic technology. Such innovations highlight the transformative potential of hybrid material systems in developing next-generation solar cells that are both efficient and economically viable, paving the way for broader adoption of sustainable energy solutions [38]. Py3 is the primary molecule of our SAMS cluster, with certain modifications made in the shaded area of Fig. 1 a), which is in contact with the perovskite layer. The stable modifications can be seen in Fig. 1(b), they are named as follows and each olecule is marked with a letter as shown bellow.

- A - (2-(pyren-1-yl)ethyl)phosphonic acid
- B - (2-(benzo[lmn]phenanthridin-8-yl)ethyl)phosphonic acid (-)
- C - (2-(5,7-diaminopyren-1-yl)ethyl)phosphonic acid
- D - (2-(5,6-diaminopyren-1-yl)ethyl)phosphonic acid
- E - (2-(6-methylpyren-1-yl)ethyl)phosphonic acid
- F - (2-(5-aminopyren-1-yl)ethyl)phosphonic acid
- G - (2-(5-ammonia-7-aminopyren-1-yl)ethyl)phosphonic acid
- I - (2-(5-(diaminomethyl)pyren-1-yl)ethyl)phosphonic acid (+)
- J - (2-(5,7-dimethylpyren-1-yl)ethyl)phosphonic acid
- K - (2-(5-ammoniapyren-1-yl)ethyl)phosphonic acid
- L - (2-(5-amino-7-ammoniapyren-1-yl)ethyl)phosphonic acid
- M - (2-(5-(diaminomethyl)pyren-1-yl)ethyl)phosphonic acid

In the first column of molecules in Fig. 1 b), carbon atoms were attached on top of Py3, resulting in the formation of B and C. In the second column, we have D, where one carbon atom was replaced with a nitrogen atom. This is followed by E and F, which were formed by attaching nitrogen atoms on top of Py3. In the third column, NH2 and NH3 groups were added to Py3 in different positions, forming G, H, I, and J. Lastly, there are K and L modifications. Other molecule models were also calculated, but only those appearing in the figure represent the stable group of the overall number of designed molecules.

### 3.1.2. Molecule-ITO and Molecule-Perovskite interaction

After defining the molecules, we placed each of them between a Perovskite layer and an ITO layer as shown in Figure. 3.2 a). Computational optimization was made for every three-layered crystal structure in order to see how these molecules would behave as a SAM layers and also to gain more information about the interactions of every molecule with two other layers. In Figure. 3.2 we can clearly see the possibility of each case appearing and even get information about bonds and physical connections between the three layers.

From Figure. 3.2 a) it can be seen that Py3 and its modifications with carbon atoms do not really have any strong interactions with the Perovskite layer, but they do make a good bonding with the ITO layer, where B is the leading molecule, as we

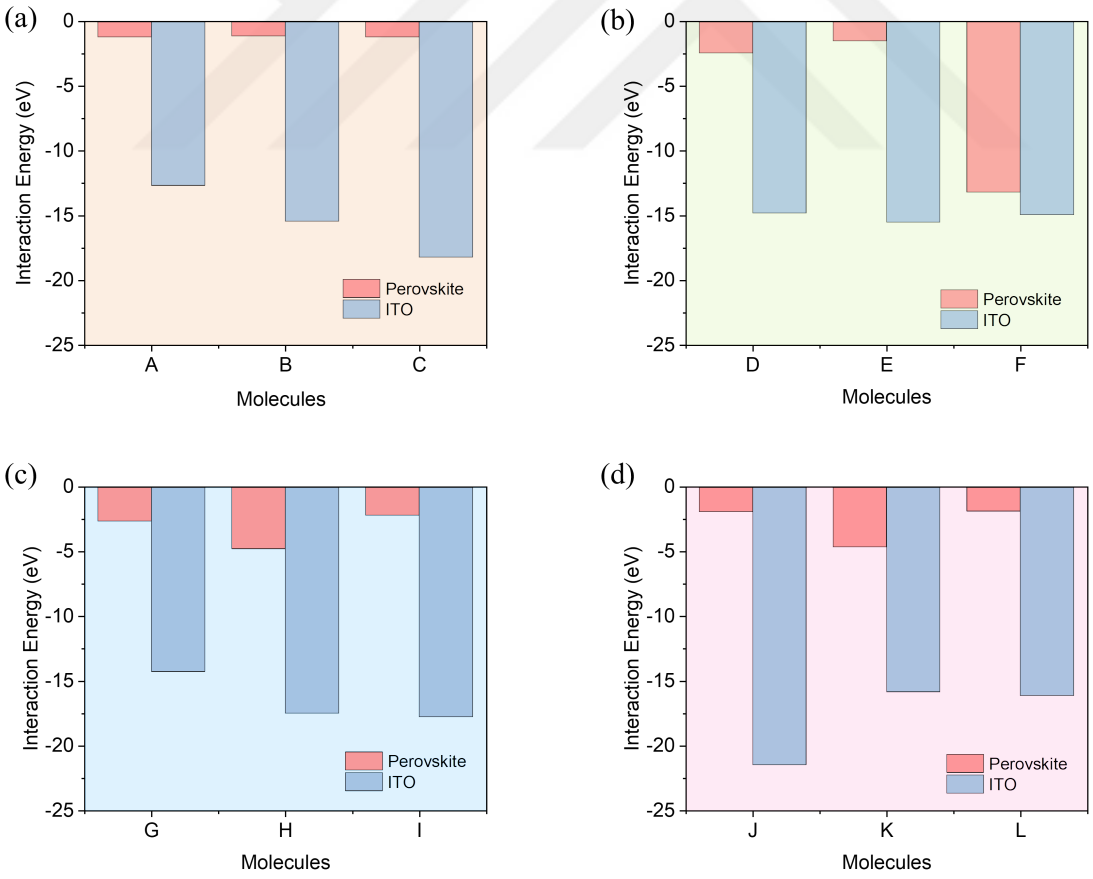


**Figure** 3.2 Shows the physical contact and binding ranges Between SAMs and Perovskite and SAMs and ITO.

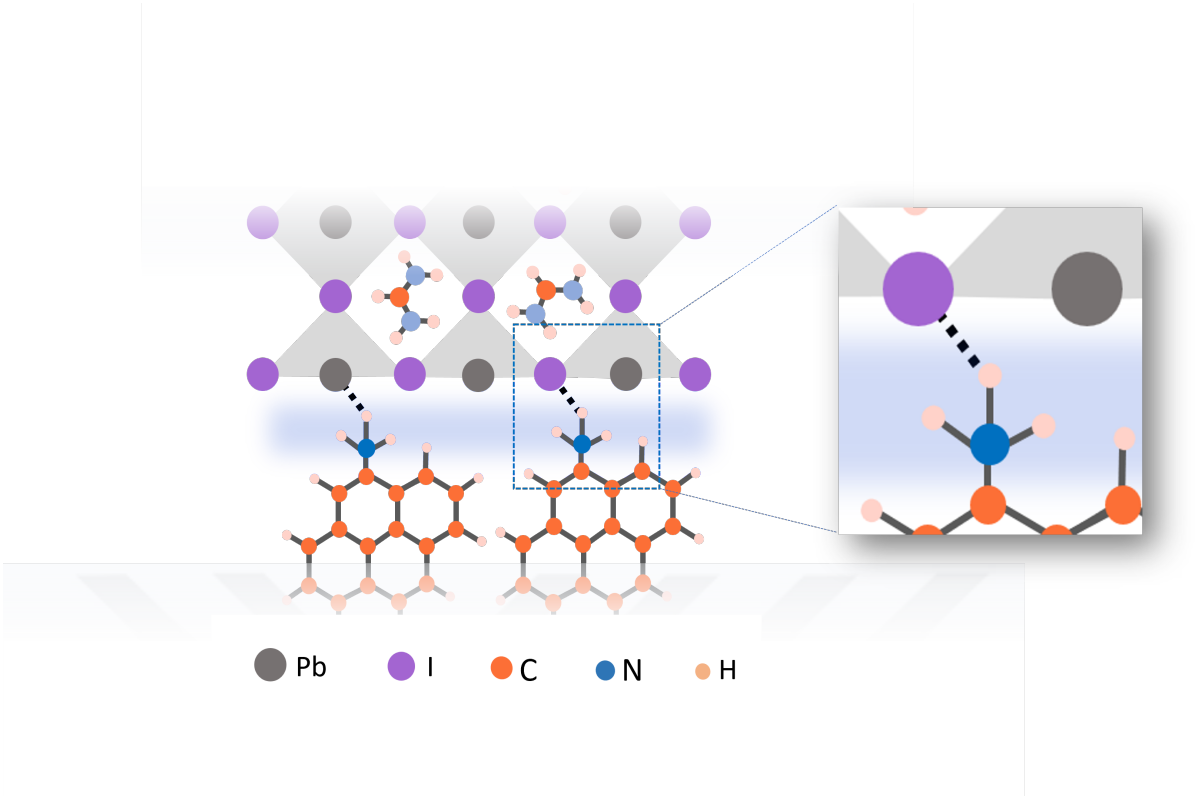


**Figure** 3.3 Represents a visual interpretation of the distace of a particular hydrogen atom with the closest Iodine atom of Perovskite layer.

know from Figure. 3.1 graph a) that the bottom part of the molecules is (2-(pyren-1-yl)ethyl)phosphonic acid and it is well known that this part of the molecule does form good bonds with ITO [39]. In graph b) it is clear that D, E, and F have similar binding energies with the ITO layer, as when it comes to the Perovskite layer D and E do have similar physical connections but F is an exception, and represents the molecule that has the most promising contact with the perovskite layer among all other molecules. K molecule Figure. 3.2 graph c) and H molecule graph d) do have better physical connections with the Perovskite layer compared to other molecules in their groups. In both of the last graphs of Figure. 3.2 all of the molecules do form good chemical bonding with the ITO layer.

We also calculated the distances between SAMs atoms and Perovskite atoms where thr physical contact was created Figure 3.4, Figure 3.5. Both figures represent the distances highlight how different parts of the same SAM molecules interact with the perovskite layer. If the atoms depicted in Figure 3.4 are closer to the perovskite

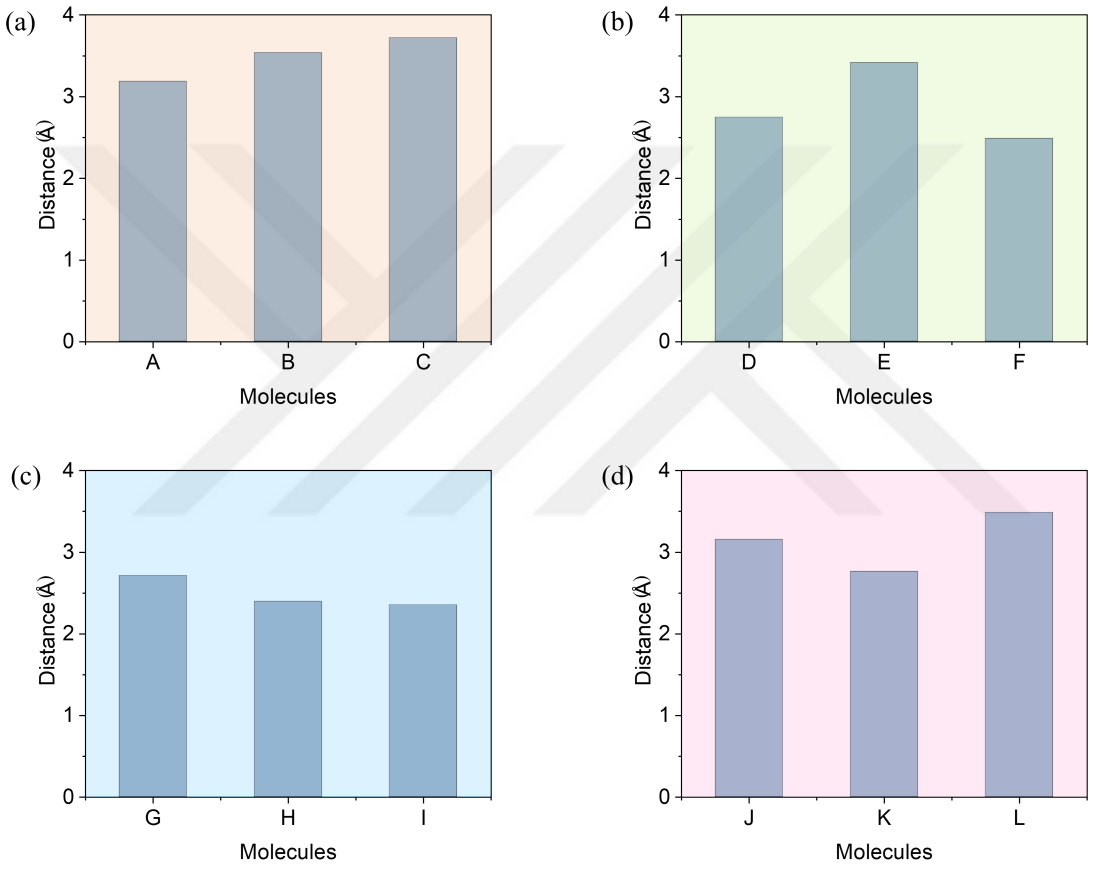


**Figure** 3.4 Shows the shortest calculated interatomic distance between all SAM layers and Perovskite layer and their comparison.

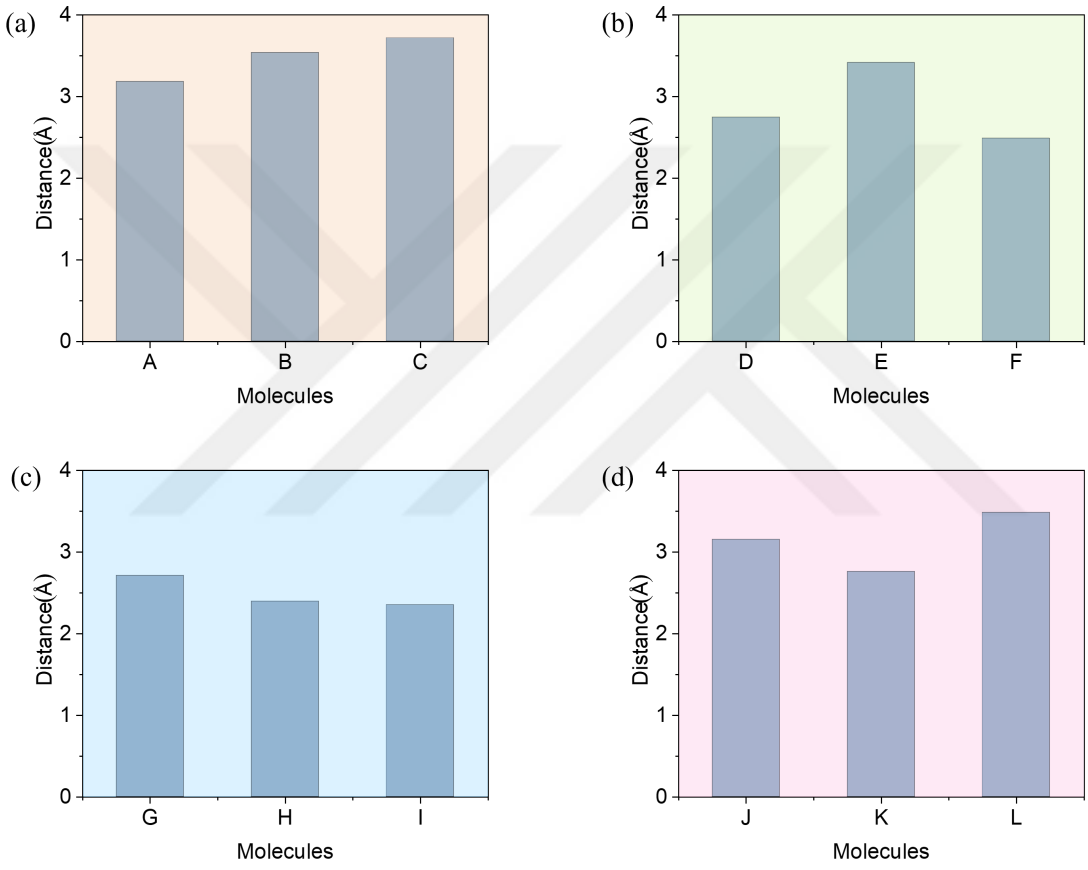


**Figure** 3.5 Shows the second shortest calculated interatomic distance between all SAM layers and Perovskite layer and their comparison.

layer compared to those in Figure 3.5, this suggests that the molecules may be tilting or bending in a way that brings certain functional groups closer to the surface while others remain further away. This conformational arrangement can significantly impact the electronic properties and the stability of the SAM/perovskite interface. The difference in distances might indicate how various functional groups within the SAM interact with the perovskite surface. For example, if the atoms in Figure 3.4 belong to functional groups designed for strong binding or charge transfer, their closer proximity to the perovskite would enhance these interactions. Meanwhile, the atoms shown in Figure 3.5 could belong to parts of the molecule that do not directly contribute to charge transfer, resulting in a greater distance from the surface.

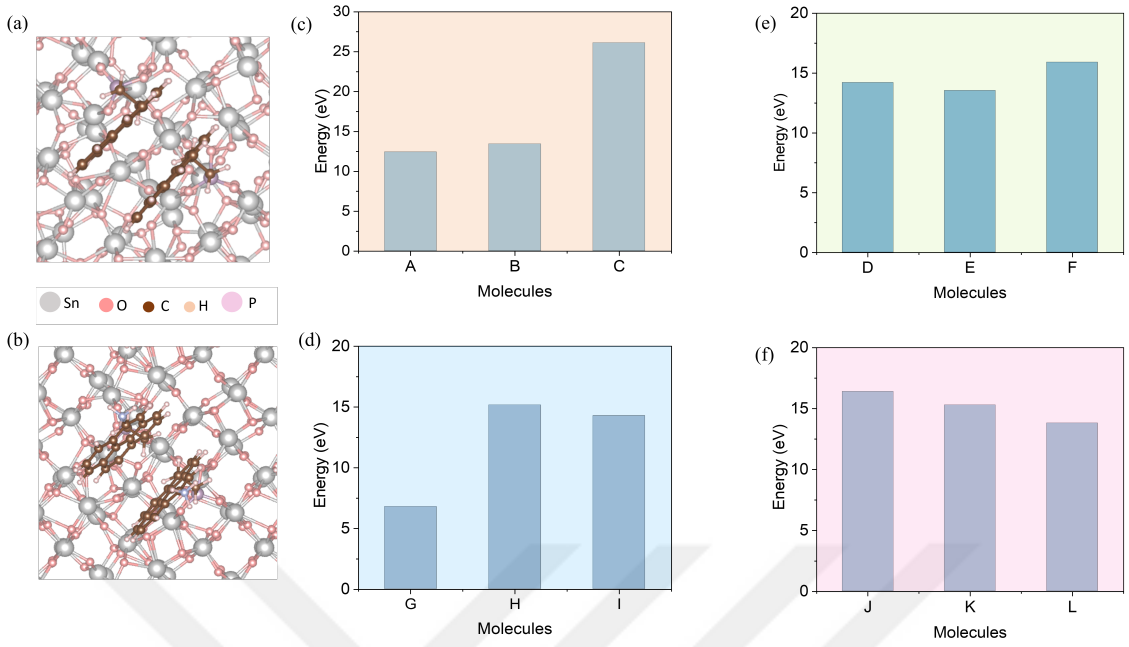


**Figure** 3.6 (a) Example image of lower stacking energy molecules,(b) Example image of higher stacking energy molecules, (c), (d), (e), (f) show the comparisons of stacking energies for each molecule within their group and betwen the groups of molecules.

### 3.1.3. Stacking Energy

As important as it is the relation between the layers the interaction between the SAM molecules themself is also quite important. In addition to studying the native stability of each molecule, we also considered if they were stable in terms of their 2D structural integrity. The core was the conjugation unit that always can drive $\pi$-$\pi$ stacking interactions between molecules and one of the essential factors for their self-assembly into well-ordered, periodic structures. The thin films stack and this stacking property is important not only because it underpins the stability of these molecules in their solid form but also as a way to order them at the molecular level.We can then have a better prediction of the performance in different applications knowing how these components interact [40]. By calculating the stacking energy of each molecule, we obtained the information shown in Figure. 3.6 In Figure. 3.6 (a) and (b) we have image examples from above of two different optimized ITO, Perovskite sandwiched SAMs molecules where in (a) image, we see two

perfectly aligned molecules which holds the meaning that these molecules have lower stacking energy a reliable case. The rest of Fig.3 shows the graphs that represent the stacking energy of each group of molecules. In image (b) we can notice that the molecules slightly repel each other, by that we can conclude that these molecules have a high stacking energy, which is not the most favorable case. Graph (c) shows stacking energy values for (A, B, C) where A has the lowest stacking energy followed by B. In graph (d) is showed the stacking energy of molecules (D, E, F) it appears that all three of them have high stacking energy in close ranges to each other, the same situation reappears in graph (e) for (J, K, L) as for graph e) from the three of molecules (G, H, I), G has the lowest stacking energy compared to , F and I.

### 3.1.4. Charge Transfer Properties

Charge density difference maps are crucial tools for visualizing and understanding the redistribution of electronic density when molecules interact with surfaces or other molecules. In the context of organic-inorganic interfaces, such as those formed between ITO and perovskite materials, CDD maps can reveal how charge is transferred across the interface, which is essential for optimizing device performance in applications like photovoltaics and optoelectronics [41]. The Figure. 3.7 represent the CDD profiles for 12 different molecules sandwiched between ITO and perovskite. These molecules act as charge transfer mediators, and the CDD maps provide insights into how their specific functional groups influence the charge distribution across the interface. By analyzing these profiles, one can determine the effectiveness of each molecule in facilitating charge transfer, which is critical for improving the efficiency and stability of devices that rely on these interfaces. The variations observed across different molecules highlight the importance of molecular design in tuning the interfacial properties for enhanced charge transport. The CDD maps provided offer valuable insights into the charge transfer characteristics of the 12 molecules studied, each positioned between ITO and perovskite. In these graphs, the larger peaks indicate regions of more significant charge transfer, which is critical for understanding the efficiency and effectiveness of each molecule as a mediator

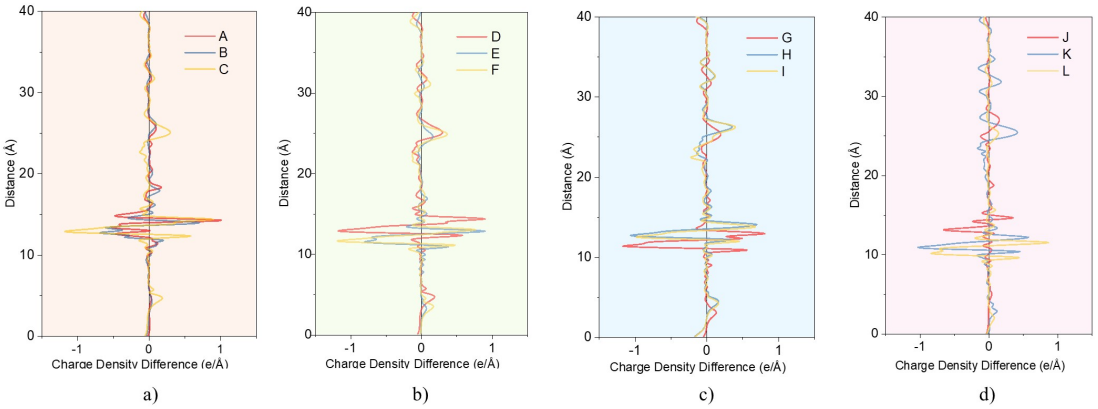


**Figure** 3.7 Provides detailed information about CTP for each molecule groups by helping us make a healthy difference between each group.

in charge transport. Figure. 3.7 Graph a) shows the CDD profiles for molecules with varying alkyl groups (A, B, and D). The peaks observed in the profiles suggest that all these molecules facilitate charge transfer to some extent, but the intensity and location of the peaks differ. Notably, the molecule labeled "A" shows slightly higher peaks compared to "B" and "C," suggesting it may facilitate a more substantial charge transfer at specific distances from the ITO surface. The presence of multiple peaks along the distance axis indicates that charge redistribution occurs in distinct regions across the interface. In Graph b) the molecules with different amino groups (D, E, F) are compared. The profiles are more closely aligned with each other, but slight differences in peak height and position are evident. The "F" molecule, in particular, shows slightly higher peaks, indicating it could be the most effective among the three. CDD maps The uniformity in the shape of the peaks suggests that the charge transfer mechanism may be similar across these molecules but with varying efficiencies. Graph c) compares molecules with double amino functionalization (G, H, I). The CDD profiles here are relatively similar, with moderate peaks throughout, suggesting that these molecules are generally effective in charge transfer. However, the "G" molecule displays slightly higher peaks, especially at specific distances, indicating it might be more efficient in facilitating charge transfer compared to the other two. The presence of these consistent peaks across the molecules suggests that double amino functionalization could be a robust strategy

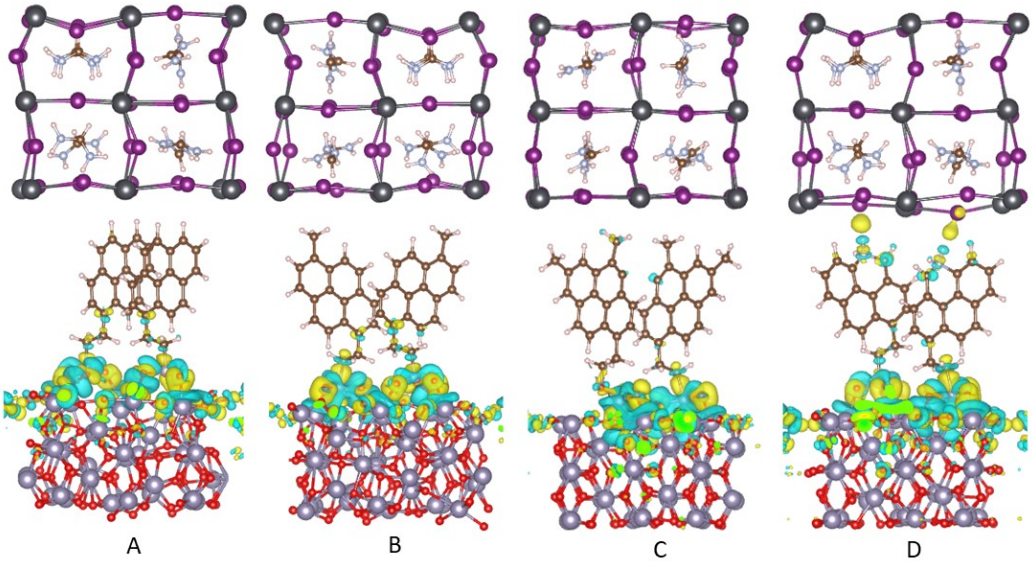


**Figure** 3.8 Charge density maps in addition to CDD graphs for molecules (A, B, C, D)

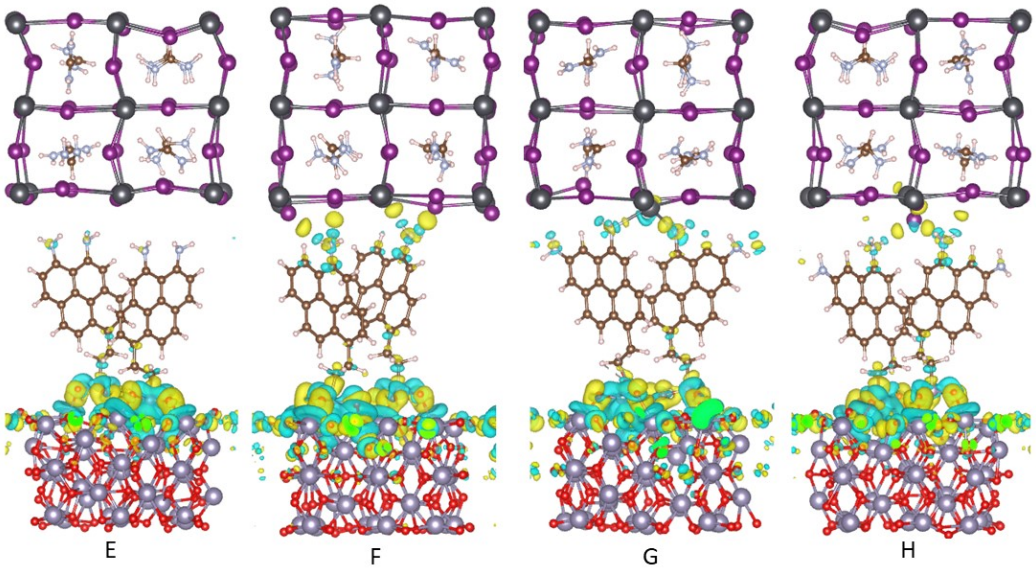


**Figure** 3.9 Charge density maps in addition to CDD graphs for molecules (E, F, G, H)

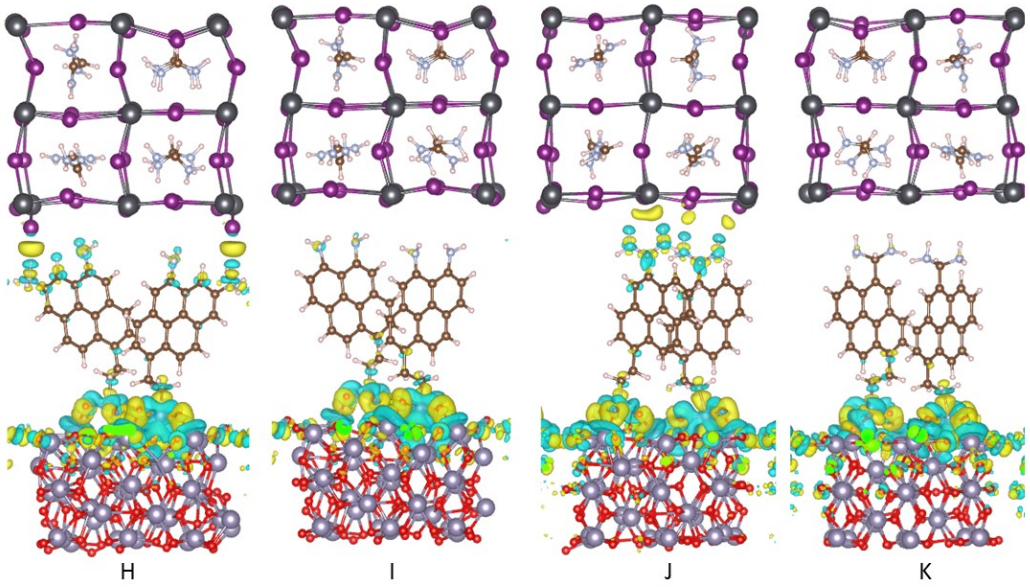


**Figure** 3.10 Charge density maps in addition to CDD graphs for molecules (H, I, J, K)

for enhancing charge transfer. Graph d): The final graph in Figure.3.7 examines the charge transfer characteristics of a parallel orientation of the G molecule (J) and formic acid in both its neutral (L) and ionized (K) forms. The CDD profiles reveal distinct charge transfer behaviors, with "K" showing the most pronounced peaks, indicating significant charge transfer. This suggests that the ionized form of formic acid is particularly effective in facilitating charge redistribution across the interface. The "J" molecule also shows notable peaks, reinforcing its potential as a good charge mediator, while the neutral formic acid (L) displays the lowest peaks, indicating lesser charge transfer activity. Overall, these CDD maps underscore the critical role of molecular design in influencing charge transfer at the ITO-perovskite interface. Molecules with larger peaks are likely more effective in facilitating charge transfer, which could lead to better performance in devices where such interfaces are key. The variation in peak intensities and distributions among the different molecules highlights the importance of functional group selection and molecular orientation in optimizing interfacial charge transfer. Figure 3.8-10 present visual CDD maps where the yellow coloured clouds represent electron clouds and blue ones rep-

resent hole clouds. From CDD maps we can clearly observe that the electron and hole clouds perfectly match CTP graphs in Figure 3.7 aligning with the fact that J molecule has better physical contact with Perovskite layer.

## 3.2. Formation of Surface Defects in Lead-Free Tin Halide Perovskites

In Figure. 3.11, Figure. 3.12, and Figure 3.13 we present defect formation energies of $FASnI_3$, $MASnI_3$, and $FAMASnI_3$ for different surface terminations. In $FASnI_3$, the defects with the lowest formation energies are $V_FA$, $Sn_FA$, $I_FA$ for the FAI surface, Sni for the I surface, and $I_i$ for the $SnI_2$ surface.In $MASnI_3$, $V_MA$, $Sn_MA$, $I_MA$ for the MAI surface, $Sn_i$ for the I surface, VI , Sni, and SnI for the $SnI_2$ surface have lowest formation energies. In $FAMASnI_3$, the defects with the lowest formation energies are $V_MA$, $Sn_MA$, $Sn_FA$, $V_FA$ for the FAMAI surface, $Sn_i$ for the surface, MASn for the $SnI_2$ surface. To sum up, the tendency of evaporation of A-site molecule causes vacancy ($V_A$) and antisite ($Sn_A$, $I_A$) defect formations in all AI (A:FA, MA, FAMA) surfaces.In all I terminations, surface iodines are ready to attract a tin ion. $SnI_2$ surface is the most defect-tolerant surface among the others since it has the highest number of positive defect formation energies. Additionally, AI surfaces have the highest number of stable defects (low DFE). Therefore, FAMAI surface is the most prone to defect formation due to being the most stable surface when compared to FAI and MAI surfaces.

Even though any point defect with low formation energy can be commonly occur in the material, further analyzes are need to identify the defect as harmful. Thus, we studied charge transitions in different growth conditions (Sn-rich, I-rich, and moderate) to reveal the influence of the defect on the electronic band structure of the material.

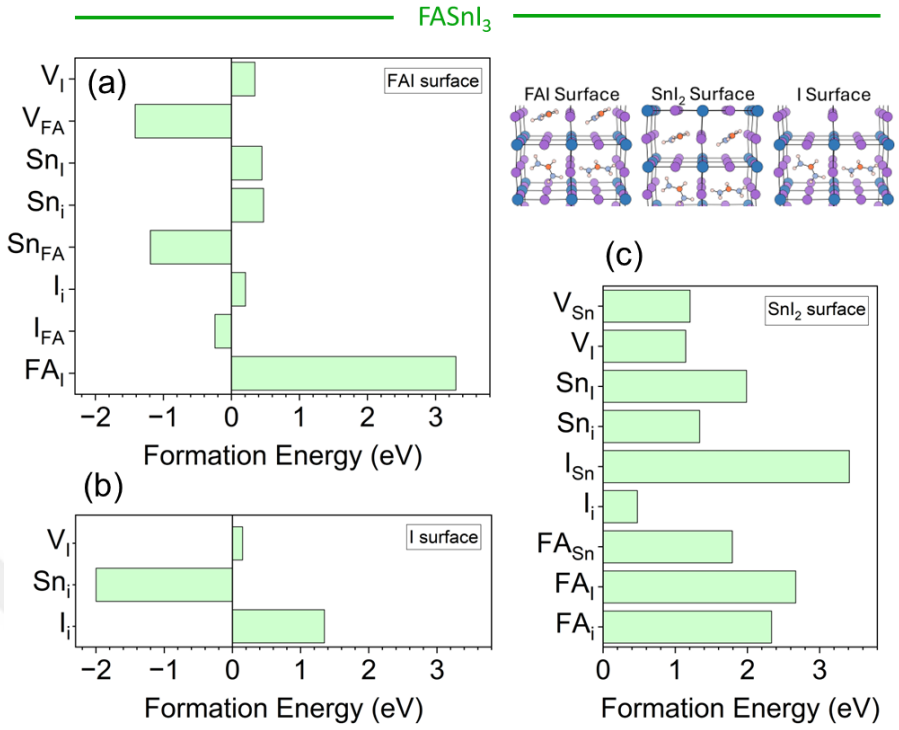


**Figure** 3.11 Formation energy of all possible intrinsic neutral point defects in (a-c) FAI, I, and SnI2 termination of FASnI3. Sn-rich growth condition is considered.

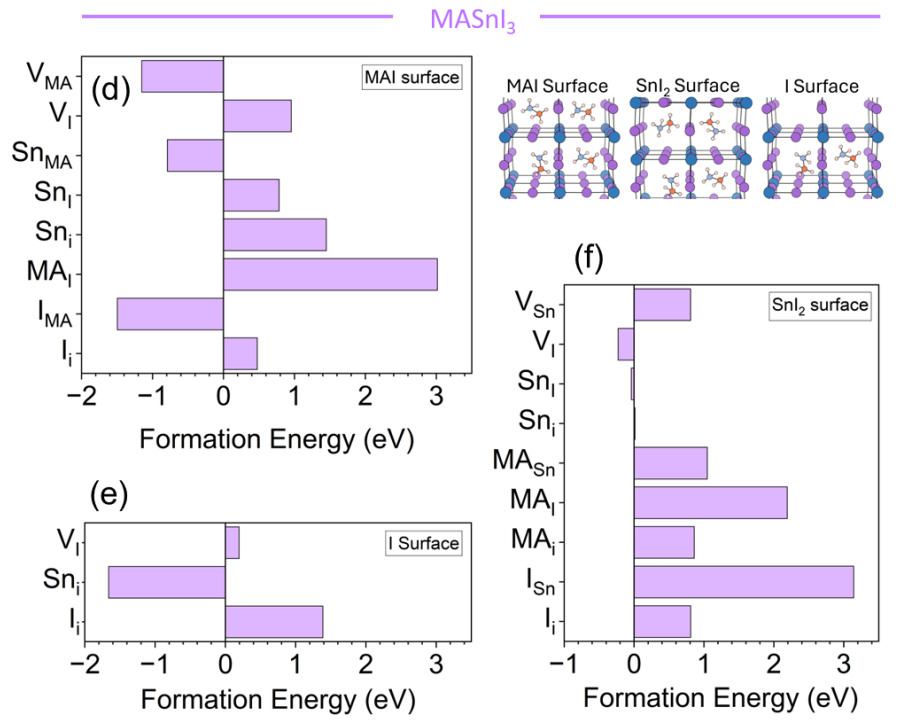


**Figure** 3.12 Formation energy of all possible intrinsic neutral point defects in (d-f) MAI, I, and SnI2 termination of MASnI3, Sn-rich growth condition is considered.

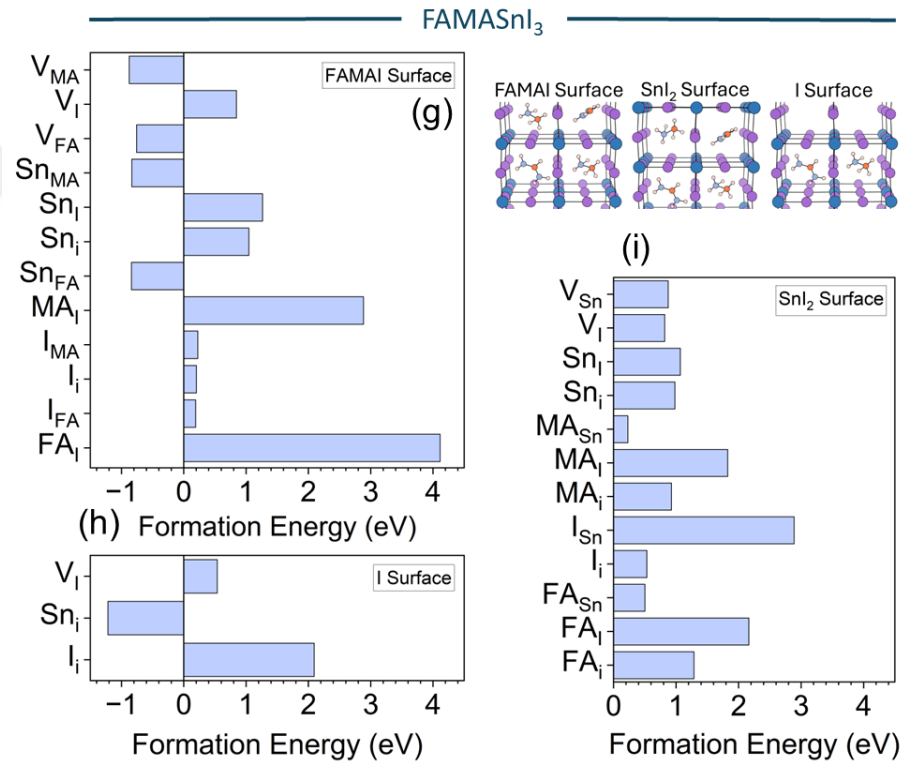


**Figure** 3.13 Formation energy of all possible intrinsic neutral point defects in (g-i) FAMAI, I, and SnI2 termination of FAMASnI3. Sn-rich growth condition is considered.

## 3.3. Publications

This thesis part of study as:

S. M. Oner, D. Acikgoz, E. Sezen, E. Latifi, E. Demiroglu, I. Yavuz, and C. Deger: Formation and Passivation of Surface Defects in Lead-Free Tin Halide Perovskites, Journal of Physical Chemistry C (under rewiew)

E. Latifi and C. Deger (in preparation): Rational Design of Self-Assembled Monolayers toward Efficient and Stable Perovskite Solar Cells

# 4. CONCLUSION

In this study, we successfully designed and investigated a series of Self-Assembled Monolayers (SAMs) for improving the performance and stability of perovskite solar cells. We also studied, defect formation in $FASnI_3$, MASnI3, and $FAMASnI_3$ varies with surface termination, with AI surfaces prone to vacancies and antisite defects. The $SnI_2$ surface is the most defect-tolerant, while FAMAI is most susceptible to defect formation. Further analysis is needed to determine the impact of these defects on the material's electronic properties. Through detailed computational modeling, abot the SAMs part we explored the interactions between various modified Py3 molecules, the perovskite layer, and the ITO substrate. Our findings indicate that specific molecular modifications can significantly enhance the bonding and charge transfer efficiency at the perovskite/SAM/ITO interface, which is crucial for the device's overall efficiency. Notably, molecules like B, D, F, K, and H demonstrated strong physical connections and favorable charge density distributions, particularly with the perovskite layer. The stacking energy analysis further highlighted the importance of molecular design in ensuring stable self-assembly and reducing energy losses within the SAM layer. Molecules with lower stacking energies showed better alignment and stability, crucial for forming a well-ordered SAM structure. Charge Density Difference maps revealed distinct charge transfer behaviors across different SAM molecules, emphasizing the role of functional groups in tuning the interfacial properties. Molecules such as "A," "J," and "K" exhibited enhanced charge transfer characteristics, suggesting their potential for optimizing device performance. This aspect is particularly important for the development of environmentally friendly and sustainable photovoltaic technologies. Overall, this study presents a comprehensive analysis of SAMs in perovskite solar cells, offering insights into how molecular modifications can be leveraged to improve device efficiency and stability. These findings pave the way for future developments in photovoltaic technology, where precise molecular engineering can lead to the creation of more efficient and durable solar cells, particularly in the context of lead-free tin halide perovskites.

# REFERENCES


[1] H. Canton, "International energy agency—iea," in *The Europa Directory of International Organizations 2021*, pp. 684–686, Routledge, 2021.

[2] M. Perez and R. Perez, "Update 2022–a fundamental look at supply side energy reserves for the planet," *Solar Energy Advances*, vol. 2, p. 100014, 2022.

[3] V. Masson-Delmotte, P. Zhai, A. Pirani, S. L. Connors, C. Péan, S. Berger, N. Caud, Y. Chen, L. Goldfarb, M. Gomis, *et al.*, "Climate change 2021: the physical science basis," *Contribution of working group I to the sixth assessment report of the intergovernmental panel on climate change*, vol. 2, no. 1, p. 2391, 2021.

[4] N. S. Lewis and D. G. Nocera, "Powering the planet: Chemical challenges in solar energy utilization," *Proceedings of the National Academy of Sciences*, vol. 103, no. 43, pp. 15729–15735, 2006.

[5] M. A. Green, A. Ho-Baillie, and H. J. Snaith, "The emergence of perovskite solar cells," *Nature photonics*, vol. 8, no. 7, pp. 506–514, 2014.

[6] S. Ghosh, S. Mishra, and T. Singh, "Antisolvents in perovskite solar cells: importance, issues, and alternatives," *Advanced materials interfaces*, vol. 7, no. 18, p. 2000950, 2020.

[7] Y. Zhou, F. Lu, T. Fang, D. Gu, X. Feng, T. Song, and W. Liu, "A brief review on metal halide perovskite photocatalysts: History, applications and prospects," *Journal of Alloys and Compounds*, vol. 911, p. 165062, 2022.

[8] M. A. Green and A. Ho-Baillie, "Perovskite solar cells: the birth of a new era in photovoltaics," *ACS Energy Letters*, vol. 2, no. 4, pp. 822–830, 2017.

[9] N.-G. Park, "Halide perovskite photovoltaics: History, progress, and perspectives," *MRS Bulletin*, vol. 43, no. 7, pp. 527–533, 2018.

[10] S.-W. Lee, S. Bae, D. Kim, and H.-S. Lee, "Historical analysis of high-efficiency, large-area solar cells: toward upscaling of perovskite solar cells," *Advanced Materials*, vol. 32, no. 51, p. 2002202, 2020.

[11] T. Dai, Q. Cao, L. Yang, M. H. Aldamasy, M. Li, Q. Liang, H. Lu, Y. Dong, and Y. Yang, "Strategies for high-performance large-area perovskite solar cells toward commercialization," *Crystals*, vol. 11, no. 3, p. 295, 2021.

[12] E. A. R. Assirey, "Perovskite synthesis, properties and their related biochemical and industrial application," *Saudi Pharmaceutical Journal*, vol. 27, no. 6, pp. 817–829, 2019.

[13] A. Alberti, E. Smecca, S. Valastro, I. Deretzis, G. Mannino, C. Bongiorno, G. Fisicaro, and A. La Magna, "Perovskite solar cells from the viewpoint of innovation and sustainability," *Physical Chemistry Chemical Physics*, vol. 24, no. 36, pp. 21549–21566, 2022.

[14] S. Y. Kim, S. J. Cho, S. E. Byeon, X. He, and H. J. Yoon, "Self-assembled monolayers as interface engineering nanomaterials in perovskite solar cells," *Advanced Energy Materials*, vol. 10, no. 44, p. 2002606, 2020.

[15] S. Zhang, R. Wu, C. Mu, Y. Wang, L. Han, Y. Wu, and W.-H. Zhu, "Conjugated self-assembled monolayer as stable hole-selective contact for inverted perovskite solar cells," *ACS Materials Letters*, vol. 4, no. 10, pp. 1976–1983, 2022.

[16] Y. Bai, Q. Dong, Y. Shao, Y. Deng, Q. Wang, L. Shen, D. Wang, W. Wei, and J. Huang, "Enhancing stability and efficiency of perovskite solar cells with crosslinkable silane-functionalized and doped fullerene," *Nature communications*, vol. 7, no. 1, p. 12806, 2016.

[17] Y. Zhao and K. Zhu, "Organic–inorganic hybrid lead halide perovskites for optoelectronic and electronic applications," *Chemical Society Reviews*, vol. 45, no. 3, pp. 655–689, 2016.

[18] J.-P. Correa-Baena, M. Saliba, T. Buonassisi, M. Grätzel, A. Abate, W. Tress, and A. Hagfeldt, "Promises and challenges of perovskite solar cells," *Science*, vol. 358, no. 6364, pp. 739–744, 2017.

[19] M. M. Byranvand, W. Zuo, R. Imani, M. Pazoki, and M. Saliba, "Tin-based halide perovskite materials: properties and applications," *Chemical Science*, vol. 13, no. 23, pp. 6766–6781, 2022.

[20] P. Hohenberg and W. Kohn, "Inhomogeneous electron gas," *Physical review*, vol. 136, no. 3B, p. B864, 1964.

[21] W. Kohn and L. J. Sham, "Self-consistent equations including exchange and correlation effects," *Physical review*, vol. 140, no. 4A, p. A1133, 1965.

[22] J. P. Perdew and K. Schmidt, "Jacob's ladder of density functional approximations for the exchange-correlation energy," in *AIP Conference Proceedings*, vol. 577, pp. 1–20, American Institute of Physics, 2001.

[23] A. J. Cohen, P. Mori-Sánchez, and W. Yang, "Insights into current limitations of density functional theory," *Science*, vol. 321, no. 5890, pp. 792–794, 2008.

[24] A. Corcor, "Formation alkali metal doped hybrid peovskites," *Marmara Üniversitesi Fen Bilimleri Enstitüsü*, pp. 7–12, 2024.

[25] G. Kresse and J. Hafner, "Ab initio molecular dynamics for liquid metals," *Physical review B*, vol. 47, no. 1, p. 558, 1993.

[26] G. Kresse and J. Furthmüller, "Efficiency of ab-initio total energy calculations for metals and semiconductors using a plane-wave basis set," *Computational materials science*, vol. 6, no. 1, pp. 15–50, 1996.

[27] J. P. Perdew, A. Ruzsinszky, G. I. Csonka, O. A. Vydrov, G. E. Scuseria, L. A. Constantin, X. Zhou, and K. Burke, "Restoring the density-gradient expansion for exchange in solids and surfaces," *Physical review letters*, vol. 100, no. 13, p. 136406, 2008.

[28] A. V. Krukau, O. A. Vydrov, A. F. Izmaylov, and G. E. Scuseria, "Influence of the exchange screening parameter on the performance of screened hybrid functionals," *The Journal of chemical physics*, vol. 125, no. 22, 2006.

[29] T. Das, G. Di Liberto, and G. Pacchioni, "Density functional theory estimate of halide perovskite band gap: When spin orbit coupling helps," *The Journal of Physical Chemistry C*, vol. 126, no. 4, pp. 2184–2198, 2022.

[30] W. Geng, L. Zhang, Y.-N. Zhang, W.-M. Lau, and L.-M. Liu, "First-principles study of lead iodide perovskite tetragonal and orthorhombic phases for photovoltaics," *The Journal of Physical Chemistry C*, vol. 118, no. 34, pp. 19565–19571, 2014.

[31] A. Srivastava, J. A. K. Satrughna, M. K. Tiwari, A. Kanwade, S. C. Yadav, K. Bala, and P. M. Shirage, "Lead metal halide perovskite solar cells: Fabrication, advancement strategies, alternatives, and future perspectives," *Materials Today Communications*, vol. 35, p. 105686, 2023.

[32] Z. Zhang, Y. Liu, Q. Sun, H. Ban, Z. Liu, H. Yu, X. Li, L. Dai, W. Yang, Y. Shen, *et al.*, "The importance of elemental lead to perovskites photovoltaics," *Chemistry of Inorganic Materials*, vol. 1, p. 100017, 2023.

[33] K. Sekar, R. Manisekaran, O. M. Nwakanma, and M. Babudurai, "Significance of formamidinium incorporation in perovskite composition and its impact on solar cell efficiency: A mini-review," *Advanced Energy and Sustainability Research*, p. 2400003, 2024.

[34] L. De Marco, G. Nasti, A. Abate, and A. Rizzo, "Perovskite single-crystal solar cells: advances and challenges," *Solar RRl*, vol. 6, no. 7, p. 2101085, 2022.

[35] Z. Zhang, R. Zhu, Y. Tang, Z. Su, S. Hu, X. Zhang, J. Zhang, J. Zhao, Y. Xue, X. Gao, *et al.*, "Anchoring charge selective self-assembled monolayers for tin–lead perovskite solar cells," *Advanced Materials*, vol. 36, no. 18, p. 2312264, 2024.

[36] M. G. Mason, L. S. Hung, C. W. Tang, S. Lee, K. W. Wong, and M. Wang, "Characterization of treated indium–tin–oxide surfaces used in electroluminescent devices," *Journal of Applied Physics*, vol. 86, no. 3, pp. 1688–1692, 1999.

[37] Y. Jin, H. Feng, Z. Fang, H. Zhang, L. Yang, X. Chen, Y. Li, B. Deng, Y. Zhong, Q. Zeng, *et al.*, "Efficient and stable monolithic perovskite/silicon tandem solar cells enabled by contact-resistance-tunable indium tin oxide interlayer," *Advanced Materials*, p. 2404010, 2024.

[38] T. Dilbeck and K. Hanson, "Molecular photon upconversion solar cells using multilayer assemblies: progress and prospects," *The Journal of Physical Chemistry Letters*, vol. 9, no. 19, pp. 5810–5821, 2018.

[39] W. Jiang, M. Liu, Y. Li, F. R. Lin, and A. K.-Y. Jen, "Rational molecular design of multifunctional self-assembled monolayers for efficient hole selection and buried interface passivation in inverted perovskite solar cells," *Chemical Science*, vol. 15, no. 8, pp. 2778–2785, 2024.

[40] R.-F. Dou, X.-C. Ma, L. Xi, H. L. Yip, K. Y. Wong, W. M. Lau, J.-F. Jia, Q.-K. Xue, W.-S. Yang, H. Ma, *et al.*, "Self-assembled monolayers of aromatic thiols stabilized by parallel-displaced $\pi$- $\pi$ stacking interactions," *Langmuir*, vol. 22, no. 7, pp. 3049–3056, 2006.

[41] K. B. Wiberg, C. M. Hadad, T. J. LePage, C. M. Breneman, and M. J. Frisch, "Analysis of the effect of electron correlation on charge density distributions," *The Journal of Physical Chemistry*, vol. 96, no. 2, pp. 671–679, 1992.